Egyptian Knowledge Bank
https://ijmti.journals.ekb.eg/

International Journal of Materials Technology and Innovation
Volume 3, Issue 3 (2023), pages 33-42

Online ISSN 2682-4299

Evaluation of Corrosion Resistance of GTAW API 5L X60 Steel / 2205 Duplex Stainless Steel Dissimilar Welds Produced with Different Heat Inputs

Darlington Ekeh[1], Atinuke Oladoye[1*], Lawrence Osoba[1] and Hakeem Amuda[1]

[1]Department of Metallurgical and Materials Engineering, University of Lagos, Lagos, Nigeria, 101017

*Corresponding author: E-mail: aoladoye@unilag.edu.ng (Atinuke Oladoye)

Received 31 October 2023
Accepted 16 December 2023
Published 31 December 2023

Abstract

In the present study, API 5L X60 / 2205 DSS dissimilar weld joints were fabricated using gas tungsten arc welding (GTAW) with ERNiCrMo-3 as the filler-metal. The influence of welding heat input (low (0.73 - 0.88 kJ/mm), medium (1.3 - 1.7 kJ/mm), and high (2.1 - 2.8 kJ/mm) on the resistance of the welded joints to corrosion was investigated. The pitting corrosion resistance of the welded joint was assessed using ASTM G48 immersion test. Electrochemical impedance spectroscopy, potentiodynamic polarisation, and cyclic polarisation were further employed to evaluate the corrosion resistance of the fusion zone of the welded joints in 3.5 wt. % NaCl solution. The result showed that welded joints produced at a medium heat input range exhibited the highest resistance to pitting and uniform corrosion. On the other hand, welded joints produced at high heat input exhibited the lowest corrosion resistance. These results were discussed in light of passivity of the fusion zone of the welded joints and the presence of secondary phase precipitates in its microstructures.

Keywords: Dissimilar welding, duplex stainless steels, API steels, corrosion resistance. compositions, precipitates.

1. Introduction

Dissimilar welded joints are widely employed in applications requiring a transition in material requirements from one service point to another. In the oil and gas industry, for instance, high strength low alloy (HSLA) steels are used as oil and gas transmission pipelines, but these steels are subject to corrosion in the aggressive chloride environments typically encountered in the offshore process areas. Hence, HSLA steel is replaced with more corrosion-resistant duplex stainless steel (DSS) along the flow lines and gas export lines in the splash zone [1-5].

The performance of such dissimilar welded joints in service is, however, dependent on the welding process and parameters. Amongst the welding parameters in any welding process, heat input is one of the critical factors that affect the cooling rate of the weldment as such it directly influences the microstructure of the weld zone and heat affected zone (HAZ), which in turn determines the mechanical properties and corrosion resistance of such joints [5,6].

The influence of heat input on mechanical properties of welded joint duplex SS /low alloyed steels has been the subject of numerous research [7-13], however, the influence of such on the corrosion resistance of these joints has been scarcely investigated. It is generally reported that for DSS/HSLA welds fabricated with duplex SS filler metal, high heat input promotes an increase in the austenite content of the weld, which enhances mechanical properties, while low heat input promotes high ferrite content in the weld and HAZ side of the DSS base metal, which deteriorates mechanical properties [5-9, 11, 12]. Nevertheless, the effect of heat input on the corrosion resistance of such joints have been rarely reported. For DSS/low alloy steel joints fabricated with Ni- based fillers, fewer studies have been reported in the literature: Barnhouse and Lippoids

IJMTI vol. 3, issue 3 (2023) 33-42 https://doi.org/ 10.21608/IJMTI.2023.241794.1095

[12] reported that increasing heat input enhanced toughness, impact strength and pitting corrosion resistance of DSS/Inconel 625/A26 carbon steel. The present authors recently reported that increasing welding heat input deteriorated tensile strength and yield strength and had no effect on hardness profile of the joint [13]. Apart from Ref [12], which was a comparison of mechanical and pitting corrosion resistance of DSS2205/A26 carbon steel made with duplex SS or Ni-based filler, there have been no systematic studies on the effect of heat input on the corrosion resistance of DSS/Ni-based filler/HSLA joints.

Hence, the aim of the present study was to investigate the influence of heat input on the pitting corrosion resistance of DSS/HSLA joint produced with gas tungsten arc welding (GTAW) process using ERNiCrMo-3 as the filler metal. The welded joints were produced with three different heat input ranges designated as low (0.73 - 0.88 kJ/mm), medium (1.3 - 1.7 kJ/mm) and high (2.1 - 2.8 kJ/mm) and the corrosion resistance of the welds in chloride environments using ASTM G48 immersion test in addition to electrochemical impedance spectroscopy, potentiodynamic and cyclic polarisation was investigated and discussed.

2. Material and methods

2.1 Materials and welding process

The base materials used in this study were HSLA and DSS steels commercially available as API 5L X60 and UNS32205, respectively. The base materials were obtained in cylindrical form (pipe) and had diameter of 5 mm respectively. The electrode employed for welding process was ERNiCrMo-3 electrodes with diameter 2.4 mm. Details of the composition of the materials and welding process have been described elsewhere [13].

In summary, the base metals were cut and fitted using standard V- groove butt weld configurations at an angle 30 ° to obtain a single V-groove of 60 ° with a 1 mm root face and 2.5 mm root gap as schematically shown in Fig. 1. The welding process adopted for welding was Gas tungsten arc welding (GTAW) process with direct current electrode negative (DCEN) polarity. Pure argon gas (99.99% purity) was employed as the shielding and backing. The welds were produced in three passes as shown in Fig. 1 with welding parameters given in Table 1. Heat input was calculated with the formular, $HI = \eta \frac{V.I}{S}$ wherein HI is the heat input, η is the welding efficiency (0.6 for GTAW), V is the voltage, I is the current and S is the welding speed.

Welded joint fabricated with low heat input range of 0.73 - 0.88 kJ/mm as given in Table 1 were designated as LHR, welds produced with medium heat input range of 1.3 - 1.7 kJ/mm as MHR and those produced at high heat input range of 2.1 - 2.8 kJ/mm as HHR.

Table 1 Welding parameters used for fabricating butt welded joints.

Heat Input Range (kJ/mm)	No. of Pass	Voltage (V)	Current (A)	Travel speed (mm/min)	Heat input (kJ/mm)
Low heat Input range (LHR)	Pass 1	10.3	85.0	59.5	0.88
	Pass 2	10.3	105.0	88.3	0.73
	Pass 3	11.3	115.0	94.8	0.82
Medium heat input range (MHR)	Pass 1	10.0	67.2	25.6	1.6
	Pass 2	10.0	90.0	46.0	1.3
	Pass 3	11.0	95.0	37.5	1.7
High Heat input range (HHR)	Pass 1	10.0	55.0	11.0	2.8
	Pass 2	9.4	90.0	25.5	2.1
	Pass 3	11.0	55.0	23.0	2.6

2.2 Characterisation of the welded joint

Microstructural analysis of the base materials and the welded samples have been reported in our previous publication [13], however, the welds were further characterised in this study using an X-ray diffractometer (XRD), X-ray fluorescence analyser (XRF), and Energy dispersive X-ray spectrometer (EDX). Phase analysis of the fusion zone (FZ) of the weld samples, designated as FZ-LHR, FZ-MHR, FZ-HHR to represent fusion zone of API/DSS joint produced at low heat input range, medium heat input range and high heat input ranges respectively, was

IJMTI vol. 3, issue 3 (2023) 33-42 https://doi.org/ 10.21608/IJMTI.2023.241794.1095

conducted with a Rigaku Mini Flex 6G diffractometer using Cu Kα radiation. Elemental composition of the fusion zone of the weld samples was analysed using a commercial MiniPal 4, Pananalytical X-ray fluorescence analyser (XRF). Elemental composition of MHR was further analysed with Energy dispersive X-ray spectrometer connected to a commercial scanning electron microscope (Carl Zeiss Smart Evo 10).

2.3 Corrosion Resistance Evaluation

ASTM G48 (Method A) gravimetric test was conducted to assess the pitting corrosion resistance of the welded joints. Sectioned coupons for the test included the base metals and the fusion zone (i.e API steel/ ERNiCrMo-3 filler/DSS) and designated as LHR, MHR, HHR representing sectioned coupons of weld joints produced at low, medium, and high heat input ranges respectively. The sample surfaces were ground using 240 to 600 grit SiC papers, cleansed in water and weighed using a digital weighing balance. The samples were thereafter exposed to 6 wt. % Ferric chloride solution in a beaker for 72 hours at room temperature. On completion of the test period, the coupons were removed, rinsed, scrubbed with nylon bristle brush under running water and weighed to 0.0001g sensitivity.

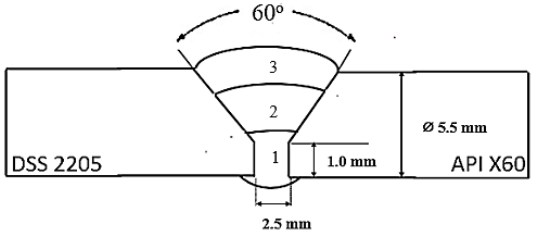

Fig. 1 Schematics of weld joint design and welding sequence

Corrosion resistance of the fusion zone of the welded joints and base metals was further investigated using electrochemical impedance spectroscopy (EIS), potentiodynamic polarisation. and cyclic polarisation techniques. All electrochemical tests were conducted using a conventional three-electrode system consisting of a saturated calomel reference electrode, a graphite rod as the counter electrode and the fusion zone (FZ) of the welded joint or base metals as the working electrodes. The working electrodes for the electrochemical test were designated as FZ-LHR, FZ-MHR, FZ-HHR to represent fusion zone of API/DSS joints produced at low heat input range, medium heat input range and high heat input range respectively. The metallic samples were embedded in epoxy resin leaving an exposed area of 100 mm^2 and afterwards grinded with different SiC paper grades. The samples were thereafter exposed to the electrolyte 3.5 wt % NaCl via a Gamry multiport corrosion cell. Open circuit measurement was conducted for 60 minutes after which EIS measurement was conducted at 10 mV from a frequency range of 10^6 to 10^{-2} Hz in potentiostatic mode. Potentiodynamic polarisation was conducted after EIS at a scan rate of 0.50 mV/s from 250 mV below open circuit potential to 1300 mV in the anodic direction. Cyclic polarisation was conducted on different fusion zone samples at 1 mV from 250 mV vs SCE below OCP to 1.5 V vs SCE for the forward scan after which the scan was reversed at the same scan rate till the current density reached 10 mA/cm^2. OCP measurements were conducted for 30 minutes before the cyclic polarisation measurements. A Gamry1000E potentiostat/Galvnostat was employed for all electrochemical tests. After the test, corroded fusion zone samples were viewed under an optical microscope (Olympus, Japan)

3. Results

3.1 XRD, XRF and EDX Characterisation of weld metal

Figure 2 shows the XRD patterns for the fusion zone of welds produced at low, medium, and high heat input hereafter designated as FZ-LHR, FZ-MHR and FZ-HHR respectively. Austenitic nickel is the major phase with niobium carbide (NbC) as a minor phase in the fusion zones, which is consistent with the optical microstructure of the welds presented in our previous study, wherein black particles were dispersed in the Ni matrix [13]. Studies [14-17] have established that these precipitates are carbides rich in Nb and Mo. It is also reported that Ni-based filler welds also contain Nb-rich laves, which are formed after the NbC precipitates. These secondary phases are common features in typical ERNiCrMo-3 filler-based welds due to the segregation of Nb and Mo during solidification. These elements then form Nb-rich Laves phase and carbides in the interdendritic region of the dendritic austenitic phase. Segregation of Nb and Mo in ERNiCrMo-3 filler-based welds according to the literature is attributed to its equilibrium distribution coefficient and dilution of base metals, which increase Fe content in the weld and reduce the solubility of these elements. Hence, as heat input increases, dilution of the ferrous base metals will increase the segregation of these elements, resulting in

IJMTI vol. 3, issue 3 (2023) 33-42 https://doi.org/ 10.21608/IJMTI.2023.241794.1095

increasing secondary phase precipitate content as shown in our previous study [13] and Kim and Lee [18].

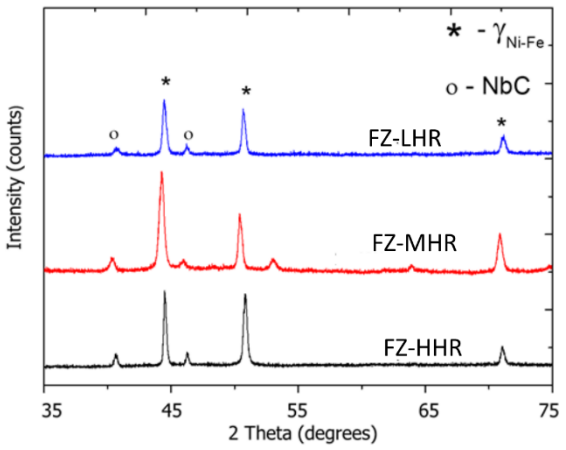

Fig. 2 XRD patterns for fusion zone sample produced at low heat input (LHR), medium heat input (MHR) and high heat input (HHR)

XRF elemental composition of FZ-LHR, FZ-MHR and FZ-HHR respectively is presented in Table 2. Ni is the highest constituent of the welds which is consistent with the XRD result. Other elements present are Cr, Nb, and Fe etc. However, XRF did not detect Mo, hence, EDX point analysis was carried out on the surface of FZ-MHR (as a representative sample) as shown in the inset of Fig 3, the results as seen in Fig. 3 evidently showed that Mo was one of the major elements in the fusion zone. Fig. 3 also confirmed the presence of Ni, Fe, Cr and Nb as obtained in the XRF analysis.

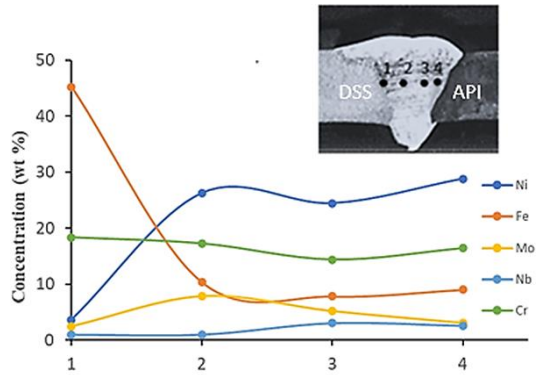

Fig. 3 EDX composition profile for fusion zone of API/DSS dissimilar weld joint produced at medium heat input (FZ-MHR)

Table 2. XRF Composition of the weldments

Material	Ni (wt. %)	Cr (wt. %)	Fe (wt. %)	Nb (wt. %)
FZ-LHR	40.26	19.64	9.09	4.31
FZ-MHR	50.72	20.35	10.27	4.03
FZ-HHR	36.78	15.51	7.79	2.52

3.2 Corrosion Resistance Evaluation

3.2.1 Pitting Immersion test

Figure 4 shows the mass loss percentage for the welded joints produced at different heat input ranges (LHR, MHR, HHR) after 72 hours of immersion in $FeCl_3$ solution. Mass loss was highest in HHR while it was lowest in MHR. Visual inspection of the samples after the test showed that corrosion occurred mostly around the HAZ and fusion line of BM-API while BM-DSS and the fusion zone samples were not corroded, and no visible pits were found on these metals. It is well known that galvanic corrosion as observed in these welded joints is due to differences in corrosion potential as will be shown in the next section.

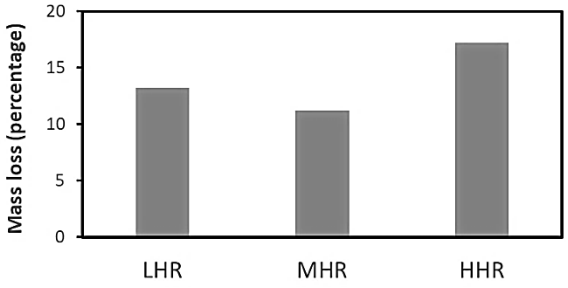

Fig. 4 Mass loss after 72 hours immersion in 6 wt. % $FeCl_3$ solution for API /DSS dissimilar welded joints produced at low heat input range (LHR), medium heat input Range (MHR) and high heat input Range (HHR).

3.2.2 Potentiodynamic Polarisation and EIS Study

The potentiodynamic polarisation plots for the base metals and the fusion zone of the welded joints (FZ-LHR, FZ-MHZ and FZ-HHR) in 3.5 wt. % NaCl solution is presented in Fig. 5. Electrochemical data obtained from the potentiodynamic plots using Tafel extrapolation method is presented in Table 3. E_{corr} is the corrosion potential, it is the thermodynamic tendency of the metals to corrode, from the E_{corr} values,

IJMTI vol. 3, issue 3 (2023) 33-42 https://doi.org/ 10.21608/IJMTI.2023.241794.1095

API steel has the lowest E_{corr} value, hence when connected to the other metals in a corrosive solution, API steels will corrode preferentially to 2205 DSS and the FZ samples as reported in the previous section. On the other hand, uniform corrosion of the base metals and FZ samples can be evaluated based on corrosion current density (i_{corr}), which is a measure of the kinetics of the corrosion process. From Table 3 corrosion resistance of the base metals and fusion zone samples in 3.5 wt. % NaCl can be ranked as DSS > FZ-MHR > FZ-LHR > API X60 ≈ FZ-HHR.

Figure 5 also shows that all samples exhibited passive behaviors except API X60. The passivity of Ni-based alloys and duplex stainless steels (DSS) is attributed to the presence of a thin surface oxide layer rich in Cr and Ni which grows on exposure to the electrolyte and prevents further dissolution [5, 19-21]. For passive metals, corrosion resistance can be evaluated using the passive current density (i_{pass}), which is a measure of the dissolution rate within the passive zone [22]. It can also be used to assess the protectiveness of the surface oxide layer. As shown in Table 3, FZ-HHR exhibited the highest i_{pass} value indicating that its passive film had the least protective properties while the passive current density of BM-DSS, FZ-LHR and FZ-MHR were comparable indicating similar dissolution rate within the passive film. EIS was further employed to evaluate the corrosion resistance of the passive films on these samples.

Figure 6 (a) and (b) show the Bode magnitude and phase angle plots for both the fusion zone of the welded joints produced at different heat input range (FZ-LHR, FZ-MHR, FZ-HHR) and the base metals respectively. Comparing the base metals and the FZ samples, BM-DSS exhibited a higher resistance than the welds as it had the highest impedance modulus |Z| value at low frequency (10^{-2} - 10^{0} Hz). On the other hand, BM-API exhibited the lowest resistance as it does not form passive film on its surface as seen in the potentiodynmaic plots. For the fusion zone samples, passive film formed on FZ-MHR had the highest impedance modulus |Z| value at low frequency implying it exhibited the highest resistance to electrolyte penetration, while the passive film formed on FZ-HHR had the lowest resistance to such phenomenon.

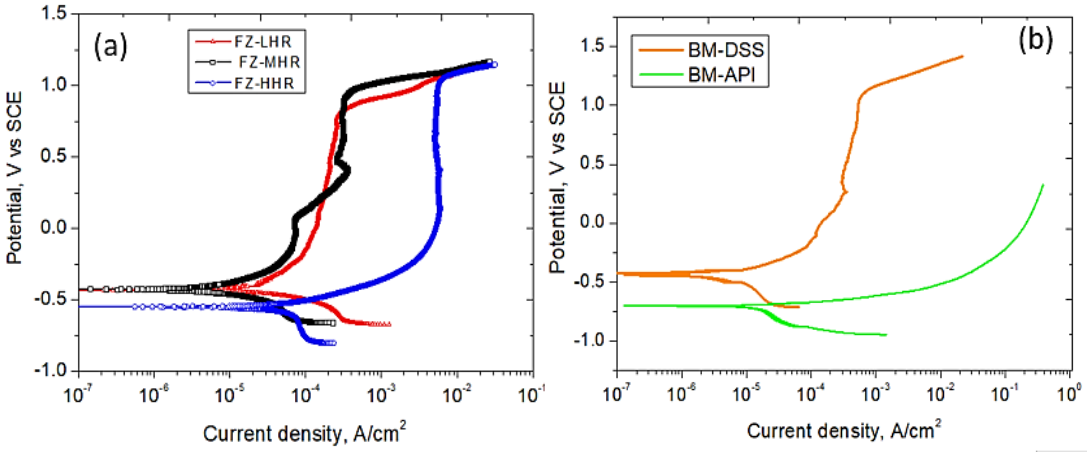

Fig. 5 Potentiodynamic polarisation curves for (a) fusion zones of API/DSS weld joints (b) base metals

Table 3. Electrochemical parameters form potentiodynamic polarisation of fusion zone of welded joint produced at low heat input range (FZ-LHR), medium heat input range (FZ-MHR), high heat input (FZ-HHR)

Material	Corrosion potential (E_{corr}, VSCE)	Corrosion current density (i_{corr}, A/cm^2)	Passive Current density (i_{pass}, A/cm^2)
FZ-LHR	- 0.430	2.63 x 10^{-5}	8.59 x 10^{-4}
FZ-MHR	- 0.425	6.69 x 10^{-6}	8. 58 x10^{-4}
FZ-HHR	- 0.550	12.50 x 10^{-5}	2.4 x 10^{-3}
BM-DSS	- 0.248	1.25 x 10^{-5}	4.17 x 10^{-4}
BM-API	- 0.704	21.74 x 10^{-5}	-

The phase angle plot in Fig. 6 (b) showed two-time constants, one at middle frequency relating to the double layer and the other at low frequency relating to the passive oxide for the passive metals. Hence, the EEC circuit in the inset of Fig 6(a) was employed to model the experimental data for BM-DSS and the fusion zone samples, however, the model in the inset of Fig. 6 (c) was used for BM-API. In the EEC model in the inset of Fig. 6 (a) Rs is the resistance of the electrolyte, R_1 represents the resistance of passive film and R_2 is the charge transfer resistance of the double layer.

The passive film is often defective and exhibits non-ideal capacitive behaviour, thus, a constant phase element (CPE) was employed instead of a capacitor. The impedance function of a CPE is given by $Z_{CPE} = Y_o^{-1}(jw)^n$ where j is the imaginary unit ($j^2 = -1$), ω the angular frequency. Y_o and n are parameters associated with the CPE. Y_o is the CPE magnitude while n is a measure of surface heterogeneity, and its values range from -1 to +1 [23]. Table 4 shows the result of fitting the model to experimental data, from the data presented the corrosion resistance of BM-DSS and fusion zone of the welded joints can be evaluated using the sum of the passive film resistance (R_1) and that of the double layer (R_2), otherwise known as polarisation resistance (R_p) [24,25]. This parameter gives the total resistance of the oxide layer to charge transport.

First, it is seen that the Rp values for BM-DSS is higher than that of the welds. Secondly, lower value of Rp for FZ-HHR (601.8 Ω.cm^2) compared to that of FZ-LHR (1841.0 Ω.cm^2) and FZ-MHR (2806.0 Ω.cm^2) implies higher ionic and electronic transport through its passive film compared to the other FZ-samples, which agrees with the high passive current density observed in the potentiodynamic polarisation result.

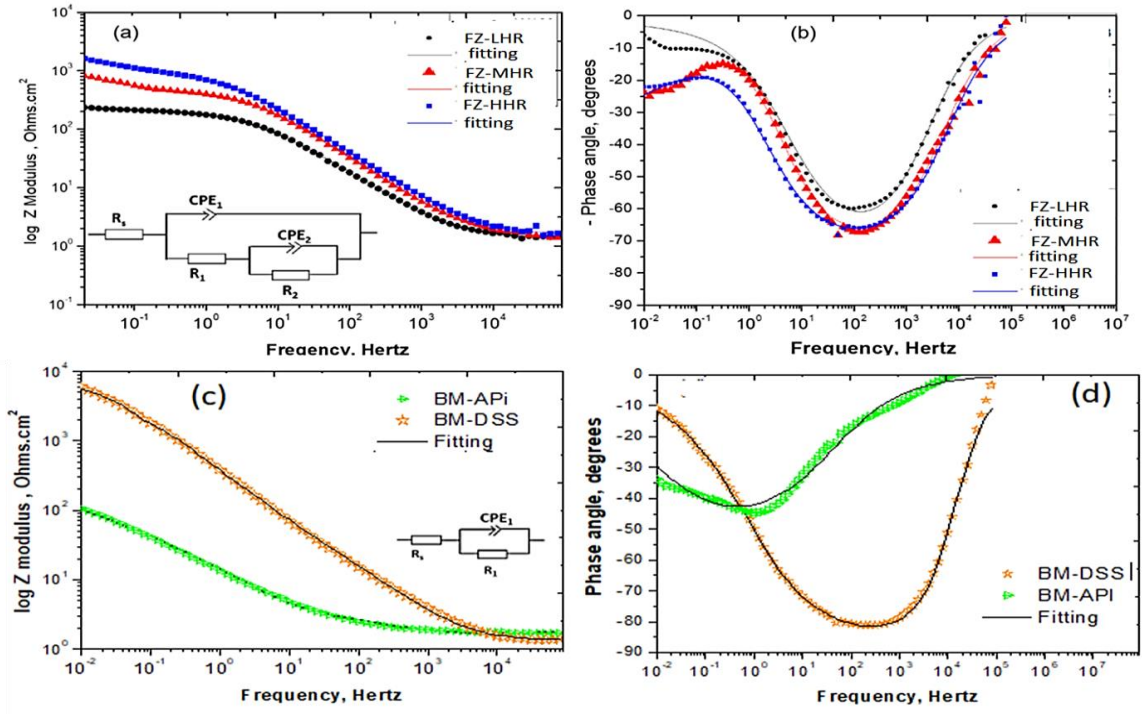

Fig. 6 (a) Bode magnitude plot (b) Phase angle plot for fusion zone of API/DSS welded joints produced at different heat input ranges (d) Bode magnitude plot (b) Phase angle plot for base metals.

IJMTI vol. 3, issue 3 (2023) 33-42 https://doi.org/ 10.21608/IJMTI.2023.241794.1095

Table 4. Electrochemical parameters obtained after fitting the EEC mode to the EIS data.

Material	R_s ($\Omega.cm^2$)	R_1 ($\Omega.cm^2$)	CPE_1 ($\mu Fcm^{-2}s^{(n-1)}$)	n_1	R_2 ($\Omega.cm^2$)	CPE_2 ($\mu Fcm^{-2}s^{(n-1)}$)	n_2
FZ-LHR	1.424	453.10	177.70	0.797	1388	7.294	0.6834
FZ-MHR	1.598	945.20	161.40	0.781	1861	3.39	0.668
FZ-HHR	1.383	204.90	396.90	0.764	56.50	92.76	1.00
BM-DSS	1.249	292.2	659.7	0.717	4933	19.74	1.00
BM-API	1.685	238.6	28.35	0.549	-	-	-

3.3 Cyclic Polarisation of Dissimilar Weld Coupons

It is well known that passive metals are susceptible to localised corrosion such as pitting corrosion. Pitting corrosion resistance of the welds was evaluated using cyclic polarisation as shown in Fig. 7. All fusion zone samples exhibited positive hysteresis loop indicating that all samples, were subject to pitting corrosion in the chloride environment. Table 5 shows the electrochemical parameters obtained from the cyclic polarisation curves in Fig. 7 wherein E_b denotes the breakdown potential and E_{rep} the re-passivation potential. The difference between these parameters, which also corresponds to the size of the hysteresis loop, can be used to assess the sensitivity of the welds to pitting corrosion [24, 26, 27]. The lower the (E_b-E_{rep}) values, the lower the sensitivity of the surface to pitting corrosion. Hence, a wider hysteresis loop for FZ-HHR as shown in Fig. 7 coupled with a higher (Eb-E_{rep}) value indicate its high susceptibility to pitting corrosion compared to other samples. To further corroborate these result, Fig. 8 (a-c) shows the micrographs of the FZ- samples taken after the cyclic polarisation test. Pits were evident in FZ -HHR compared to the other FZ samples. Fig. 8 (d), further showed that the preferential site for corrosion was the secondary Nb rich phase. Therefore, the pitting corrosion resistance of the FZ-samples is ranked FZ-MHR > FZ-LHR> FZ-HHR.

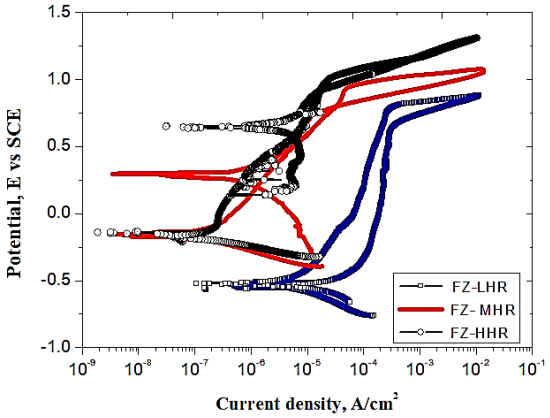

Fig. 7 (a) Cyclic polarisation curve for API/DSS welded joints produced at different heat input ranges.

Table 5. Electrochemical parameters from cyclic polarisation of FZ-samples.

Material	E_{corr} (V_{SCE})	E_b (V_{SCE})	$E_{rep.}$ (V_{SCE})	E_{b}-E_{rep} (V_{SCE})
FZ-LHR	-0.1421	0.971	0.806	-0.165
FZ-MHR	-0.1401	0.993	0.922	-0.071
FZ-HHR	-0.519	0.763	-0.522	0.241

4. Discussion

It is well known that the excellent corrosion resistance of Ni-Cr-Mo alloys, to which ERNiCrMo-3 (Inconel 625) belongs, in chloride environment is related to the presence of chromium and Mo [19-21, 22]. Chromium is primarily responsible for passivation as it forms a Cr_2O_3 oxide layer on the surface of the metal, which acts a barrier preventing dissolution by minimising electrolyte penetration. On the other hand, Mo controls re-passivation after film breakdown by inhibiting pit propagation [19, 20,22]. The protectiveness of the passive film is, however, dependent on factors like composition, microstructure of the alloy, thickness of the film etc. Composition of passive film is often analysed using advanced characterisation techniques like X-ray photoelectron spectroscopy (XPS) which is not readily available to the authors. Nonetheless, the similarity between the passive current density of FZ-LHR and FZ-MHR (Table 3) and the marginal difference observed in the size of the hysteresis loop in Fig.7 suggest that the passive film formed on these samples could have higher concentration of Cr and Mo compared to FZ-HHR samples. Studies [19-21, 22] have shown that the difference in passive current density is mainly related to the chromium content of the alloy, with higher Cr content alloys exhibiting lower passive current density,

IJMTI vol. 3, issue 3 (2023) 33-42 https://doi.org/ 10.21608/IJMTI.2023.241794.1095

which is consistent with the XRF composition wherein FZ-LHR and FZ-MHR had similar chromium content of 19.64 wt. % Cr and 20.34 wt.% Cr respectively and FZ-HHR had a lower Cr content (15.51 wt.% Cr). Mishra et al. [19] demonstrated using XPS that the passive film of high Cr Ni-based alloys was enriched in higher Cr content than the ones with lower Cr content in the passive region hence they were more protective than the alloys with lower Cr content in the passive film.

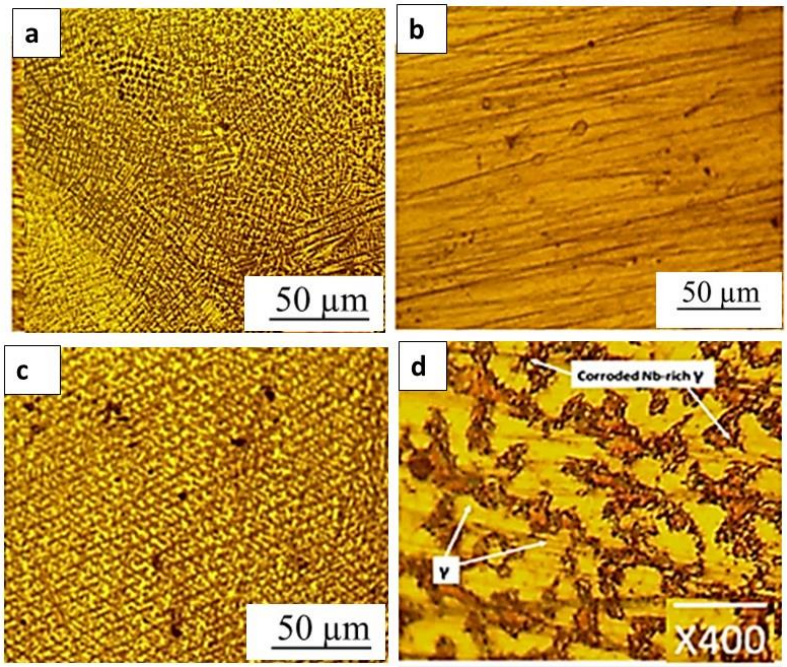

Fig. 8 Optical micrographs of fusion zone of weld joint produced at low heat input range (FZ-LHR), medium heat input range (FZ-MHR), high heat range (FZ-HHR) after cyclic polarisation.

A similar trend of higher Mo content in the passive film leading to higher protectiveness in chloride environment was also observed for Mo content. The results obtained in this study is consistent with these previous studies and could justify the differences in passive behaviour between the FZ-samples observed in the EIS and potentiodynamic polarisation results. It is, however, noted that the FZ-samples in this study are welded samples and not wrought samples used in Ref [19-22], hence, the presence of a secondary phase in the microstructure of the welded alloys used in the study will play a significant role in the protectiveness of the passive film.

The XRD patterns of the fusion zone samples combined with their microstructure presented in Ref [13] as well as the microstructure after cyclic polarisation presented in Fig. 8(d) showed that the fusion zone samples essentially consisted of an austenitic matrix with NbC and Laves phase as the secondary phase precipitates. Studies [24, 28-31] have shown that these secondary phase precipitates are rich in Nb and Mo but deficient in Cr and Ni. Chromium is the main element for passivation, therefore, deficiency in Cr implies that passivation will be difficult on these secondary phases hence a non-uniform film, which will be prone to chloride attack, will be formed [13,33-35]. Alano et al. [29] had shown that increase in secondary phase precipitates will results in a more defective and porous passive film compared to that formed on samples with lower second phase precipitates. The defective and porous nature of the passive film makes it more susceptible to pitting corrosion.

Hence, the higher current density and lower polarisation resistance (Rp) of the passive film on FZ-HHR in the potentiodynamic and EIS result respectively is attributed to the increase in secondary phase precipitates in FZ-HHR compared to the other samples as shown in the microstructure of the FZ-samples presented in Ref [13]. Also, the similarities between the passive current density of FZ-LHR and FZ-MHR as well as the corrosion potential suggest that the difference in concentration of second phase precipitates in these samples may be marginal.

IJMTI vol. 3, issue 3 (2023) 33-42 https://doi.org/ 10.21608/IJMTI.2023.241794.1095

It has also been reported that compositional variation between the matrix and secondary phase precipitate leads to a difference in the electrode potential thereby promoting galvanic corrosion between the precipitate and the austenitic Ni matrix wherein the secondary phase precipitate dissolves preferentially to the matrix [30,31]. Optical micrograph of FZ-HHR taken after the cyclic polarisation (Fig.8 (d)) is consistent with the work of these authors, wherein the austenitic Ni matrix is intact but the interdendritic regions which contain the second phase precipitates was corroded.

5. Conclusion

Th In this study, the corrosion resistance of gas tungsten arc welded API 5L X60 / 2205 DSS joints produced under low, medium, and high heat input range using ERNiCrMo-3 filler metal was investigated. Based on the experimental results obtained the following conclusions were drawn:

1) Corrosion resistance evaluation of the welded joint using ASTM G-48 method A revealed that the joint produced with medium heat input exhibited the lowest corrosion rate, compared to the joints produced with low and high heat input. Mass loss was majorly around the fusion line and HAZ on the API steel side while the fusion zone and base metal DSS area were not corroded, and no pit was found on the metals.
2) Electrochemical studies of the fusion zone of the welded joints using EIS, pontentiodynamic and cyclic polarisation techniques showed that the weldment produced with high heat input was most susceptible to general and pitting corrosion. Its low corrosion resistance was attributed to its low chromium content and high second phase precipitates content which affected the uniformity of the passive film formed on its surface.
3) In designing welding procedures specifications for dissimilar weld joints of API 5L X60 and DSS 2205, medium heat input within the range of 1.3 - 1.7 kJ/mm is recommended to obtain corrosion resistant joints.

References

[1] J. Wang, M. Lu, L. Zhang, W. Chang, L. Xu, L. Hu, Effect of welding process on the microstructure and properties of dissimilar weld joints between low alloy steel and duplex stainless steel Int. J. Miner. Metall. 19 (6) (2012) 518-524.

[2] A.H. Saedi, E. Hajjari, and S.M. Sadrossadat, Microstructural characterization and mechanical properties of TIG-welded API 5L X60 HSLA steel and AISI 310s stainless steel dissimilar joints. Metallurgical and Materials Transactions, joints. Metallurgical and Materials Transactions, 49 (2018) 5497–5508.

[3] W. N. Khan, R. Chhibber, Effect of filler metal on solidification, microstructure, and mechanical properties of dissimilar super duplex/pipeline steel GTA weld, Mater. Sci. Eng. A, 803 (2021)140476.

[4] B. I. Mendoza, Z. C. Maldonado, H. A. Albiter, P. E. Robles, (2010) Dissimilar Welding of Superduplex Stainless Steel/HSLA Steel for Offshore Applications Joined by GTAW, Engineering 2(7) (2010) 520-528

[5] J. Verma, R.V Taiwade Effect of welding processes and conditions on the microstructure, mechanical properties and corrosion resistance of duplex stainless-steel weldments—A review, J. Manuf. Process 25 (2017) 134–152 https://doi.org/10.1016/j.jmapro.2016.11.003

[6] L. Han, T. Han, G. Chen, B. Wang, J. Sun, Y. Wang, Influence of heat input on microstructure, hardness and pitting corrosion of weld metal in duplex stainless steel welded by keyhole-TIG. Materials Characterization, 175 (2021) 111052. doi:10.1016/j.matchar.2021.11105

[7] M. Sadeghian, M. Shamanian, A. Shafyei, Effect of heat input on microstructure and mechanical properties of dissimilar joints between super duplex stainless steel and high strength low alloy steel. Mater. & Des. 60, (2014) 678–684

[8] Srinivasan, V. Muthupandi, W. Dietzel and V. Sivian, (2006) Microstructure and corrosion behaviour of shielded metal arc-welded dissimilar joints comprising duplex stainless steel and low alloy steel, J. Mater. Eng. Perform. 15 (6) (2006) 758 -764

[9] S. M. Zahraei, R. Dehmolaei, A. Ashrafi, The effect of heat input on microstructure and HAZ expansion in dissimilar joints between API5L X80 / DSS 2205 steels using thermal cycles, Revista de Metalurgia 58 (2) (2022).

[10] H. Tasalloti , P. Kah, J. J. Martikainen, Effect of heat input on dissimilar welds of ultra-high strength steel and duplex stainless steel: Microstructural and compositional analysis, Mater. Charact. 123 (2017) 29-41.

[11] S. Wang, Q. Ma, Y. Li, Characterization of microstructure, mechanical properties and corrosion resistance of dissimilar welded joint between 2205 duplex stainless steel and 16MnR, Mater. Des.,32(2) (2011) 831-837.

[12] E. J. Barnhouse and J.C Lippold, Microstructure /Property Relationships in Dissimilar welds between Duplex stainless steels and Carbon steels, Welding J. 77 (12) (1998) 477-487.

[13] D. Ekeh, L. Osoba, T. Lawal, M. Amuda, Microstructure and Mechanical Properties of

IJMTI vol. 3, issue 3 (2023) 33-42 https://doi.org/ 10.21608/IJMTI.2023.241794.1095

Dissimilar Welds of Duplex and API Steel for Offshore Applications, Int. J. Mater. Prod. 3 (2) (2023) 80-91.

[14] M. Tumer, T. Mert, T. Karahan, Investigation of microstructure, mechanical and corrosion behaviour of nickel based alloy 625/duplex stainless steel UNS S32205 dissimilar weldments using ERNiCrMo-3 filler metal, Weld World 65 (2021) 171-182.

[15] C. P. Alvaraes, J. C. F. Jorge, L. F.G. de Souza, L. S. Araujo, M, C. Mendes, H. N. Farneze, microstructure and corrosion properties of single layer Inconel, J. Mater. Res. Technol. 9(6) (2020) 16146 -16158

[16] J.S. Zuback, P. Moradifar, Z. Khayat, N. Alem, T.A. Palmer, Impact of chemical composition on precipitate morphology in an additively manufactured nickel base superalloy, J. Alloys Compd. 798 (2019) 446 -457

[17] C.C. Silva, V. H. C. De Albuquerque, E.M. Mina, E. P. Moura, J. O Manuel R.S. Tavares, Mechanical Properties and Microstructural Characterization of Aged Nickel-based Alloy 625, Metall. Mater. Trans. A 49 (2018) 1653-1673

[18] J-S Kim, H-Woo Lee, A Study on Effect of Intergranular Corrosion by Heat Input on Inconel 625 Overlay Weld Metal, Int. J. Electrochem. Sci., 10 (2015) 6454- 6464

[19] A.C. Lloyd, J.J. Noel, S. McIntyre, D.W. Shoesmith, Cr,Mo and W alloying additions in Ni and their effect on passivity, Electrochim. Acta 49 (2004) 3015 -3027.

[20] A.K. Mishra, N. Ebrahimi, D.W. Shoesmith and P.E. Manning, Material selection for use in Hydrochloric acid presented at CORROSION 2016, Vanocouver, Canada, 6 -10 March 2016

[21] N. Ebrahimi, M.C. Biesinger, D.W. Shoesmith, J.J. Noël, The influence of chromium and molybdenum on the repassivation of nickel-chromium-molybdenum alloys in saline solutions. Surface and Interface Analysis, 49 (13) (2017) 1359–1365.

[22] J. D. Henderson, B. A. M. Momeni, S. Anderson, V. Dehnavi, D. Zagidulin, D. W. Shoesmith, J. J. Noël Investigating the Influence of Cr and Mo Additions to Commercial NiBased Alloys Exposed to Neutral and Acidic Chloride Solutions, J. Electrochem. Soc. 167 (2020) 131512

[23] P. Roberge, Analysis simulated electrochemical impedance spectroscopy results by the systematic permutation of date points, in M.K.J. Scully, D. Silverman (Eds.) Electrochemical Impedance Analysis and Interpretation, 1st edition, ASTM International, Philadelphia ,1993, pp. 54-72, http://doi.org/10.1520/stp18063s.

[24] J. Kangazian, M. Shamanian, A. Ashraf, Dissimilar welding between SAF 2507 stainless steel and Incoloy 825 Ni-based alloy: The role of microstructure on corrosion behavior of the weld metals. J. Manufacturing Processes 29 (2017) 376-38.

[25] Z. Brytan, J. Niagaj, Corrosion studies using potentiodynamic and EIS electrochemical techniques of welded lean duplex stainless steel UNS S82441. Appl. Surf Sci 2016;388:160–8, http://dx.doi.org/10.1016/j.apsusc.2016.01.260.

[26] H.R. Zareje Rajani, S.A.A. Akbari Mousavi, F. Madani Sani, Comparison of corrosion behaviour between fusion cladded and explosive cladded Inconel 625/plain carbon steel bimetal plates, Mater. Des. 43 (2013) 467-474.

[27] U. Trdan, J. Grum, Evaluation of corrosion resistance of AA6082-T651 aluminium alloy after laser shock peening by means of cyclic polarisation and ElS methods. Corrosion Science, 59(2012) 324–333. doi:10.1016/j.corsci.2012.03.019

[28] C.P. Avaraes, J.C.F. Jorge, L.F.G de Souza, L. S. Araujo, M.C. Mendes, H. N. Farneze, Microstructure and corrosion properties of layer Inconel 625 weld cladding obtained by the electroslag welding process. J. Mater. Res. Technol. 9 (6) 2020, 16146.

[29] J.H. Alano, R. L. Siqueria, A.D. de Oliveria, G. dos S. Vacchi, C.A.D. Rovere, S. E. Kuri. Effect of TCP phase formation on the electrochemical corrosion behaviour of the nickel-based superalloy UN26455, Corro. Sci. 177 (2020) 108894.

[30] P. Guo, X. Lin, J. Xu, J. Liu, W. Huang, Electrochemical removal of different phases from laser solid formed Inconel 718, J. Electrochem. Soc. 164 (7) 2017, 151 – 157.

[31] Y. Zhang, X, Lin , J, Yu, P. Guo c, J. Li , T, Qin , J, Liu, W. Huang, Electrochemical dissolution behavior of heat treated laser solid formed Inconel718, Corro. Sci, 173, 15 (2020), 108750.